Erbium-doped GaN bulk crystals as a gain medium for eye-safe high energy lasers

Z. Y. Sun, Q. W. Wang, J. Li, J. Y. Lin[a)] and H. X. Jiang[a)]

Department of Electrical and Computer Engineering, Texas Tech University, Lubbock, TX 79409, USA

ABSTRACT

High energy lasers (HELs) operating around 1.5 μm are considered eye-safe and are highly sought-after for use in defense, industrial processing, communications, medicine, spectroscopy, imaging and various other applications where the laser is expected to travel long distances in free space. Compared to YAG, GaN has a higher thermal conductivity, lower thermal expansion coefficient, and lower temperature coefficient of the refractive index (*dn/dT*) around 1.5 μm. Hence, HELs based on erbium doped GaN (Er:GaN) are expected to outperform those based on Er:YAG in terms of average power, power density, temperature stability and beam quality. Here, we provide a brief overview on the progress made in authors' laboratory for the realization of freestanding Er:GaN wafers of 2-inches in diameter with a thickness on the millimeter scale. These freestanding wafers were obtained via growth by hydride vapor phase epitaxy (HVPE) in conjunction with a laser-lift-off process. Optical absorption and resonantly excited photoluminescence emission spectra have enabled the construction of energy level diagrams pertaining to the excitation and emission mechanisms of Er:GaN eye-safe HELs operating around 1.5 μm. The results have shown that the common excitation and emission scheme of Er:YAG is not entirely applicable to achieve Er:GaN eye-safe lasers. In addition to higher thermal conductivity of Er:GaN over Er:YAG gain medium, Er:GaN eye-safe lasers appear to possess lower quantum defects than Er:YAG lasers.

Key words: Gain medium, Erbium, solid-state lasers, high energy lasers, Er doped, GaN wide bandgap semiconductors, HVPE epitaxial growth

1. INTRODUCTION

High energy and high power solid-state lasers (SSL) operating in the "eye-safe" spectral region are highly sought-after for use in defense, industrial processing, communications, medicine, spectroscopy, imaging and various other applications where the laser is expected to travel long distances in free space. The optical gain medium is the heart of an SSL system. When doped in a host, the emission lines resulting from the intra-4f transitions from the first excited state manifold ($^4I_{13/2}$) to the ground state manifold ($^4I_{15/2}$) in Er^{3+} ions are near 1.5 μm [1, 2], which not only matches the technologically important wavelength window of minimum propagation loss in optical fibers, but also lies in the "eye-safe" region as the upper limit of eye-safe laser exposure at 1.5 μm is more than 4 orders of magnitude higher than that of the wavelengths below or close to 1 μm [3, 4]. Moreover, 1.5 μm lasers also has a high atmospheric transmittance [5]. Currently, high energy lasers (HEL) based on Er doped YAG (Er:YAG) have reached high performance levels [6-13]. However, with the relatively poor thermal properties of YAG with a thermal conductivity $\kappa \approx 14$ W/m·K and thermal expansion coefficient $\alpha \approx 8 \times 10^{-6}$ $^oC^{-1}$, the heat dissipation capability of YAG gain medium is relative poor, which limits the optical output energy, average power, as well as the beam quality [14-17]. Therefore, finding gain materials with improved thermal properties is highly desirable.

Of the wide bandgap III-nitride semiconductors which have demonstrated excellent performances in high power, high temperature electronics and optoelectronics [18-21], Er doped GaN (Er:GaN) is a very promising gain medium for HELs. Compared to YAG, GaN has a much larger thermal conductivity ($\kappa = 253$

Optical Components and Materials XV, edited by Shibin Jiang, Michel J. F. Digonnet, Proc. of SPIE Vol. 10528, 105280E
 · doi: 10.1117/12.2293166

W/m·K for GaN versus 14 W/m·K for YAG) [22], lower thermal expansion coefficient ($\alpha \approx 3.53 \times 10^{-6}$ ºC^{-1} for GaN versus 8×10^{-6} ºC^{-1} for YAG) [22], and lower temperature coefficient of the refractive index, *dn/dT* (0.7×10^{-5} ºC^{-1} for GaN versus 1.75×10^{-5} ºC^{-1} for YAG) [23]. Hence, HELs based on Er:GaN are expected to outperform those based on Er:YAG in terms of average power, power density, and beam quality.

We are investigating Er:GaN crystals as a novel gain medium for next generation solid-state HELs. Metal organic chemical vapor deposition (MOCVD) technique has been further developed and employed to synthesis Er:GaN thin films with enhanced emission efficiency at 1.5 μm [24, 25]. The MOCVD grown Er:GaN epilayers are suitable to construct optically pumped lasers in the slab (or waveguide) geometry, whereas Er:GaN bulk crystals have been synthesized via hydride vapor phase epitaxy (HVPE) growth technique with large thicknesses (>100 μm) [26-28] and ultimately these materials are to be used to construct optically pumped lasers in the disk, slab or rod form factors.

II. RESULTS AND DISCUSSION

1. Growth of Er:GaN bulk crystals by HVPE

We have carried out HVPE growth of Er:GaN crystals. The optical quality of Er:GaN crystals has been improved by monitoring the 1.54 μm emission under both near the bandgap and resonant excitation using 375 nm and 980 nm lasers [26-28].

We have successfully obtained freestanding Er:GaN bulk crystals with a thickness on the mm scale via HVPE growth together with the laser-lift-off (LLO) process. Prior to the deposition of Er:GaN by HVPE, a GaN epilayer of 3 μm in thickness was deposited on a (0001) sapphire substrate by MOCVD to serve as a template. The GaN template was then transported into an HVPE reactor for the

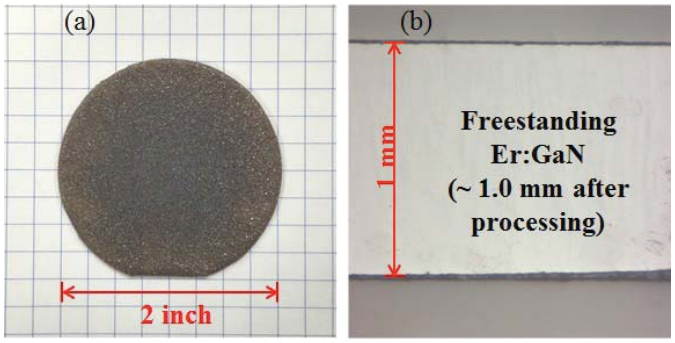

Fig. 1. (a) An optical image of a 2-inch freestanding Er:GaN wafer (1.2 mm in thickness) before polishing. (b) An optical image of a cross-sectional view of Er:GaN bulk sample [Ref. 27, reproduced with permission from Appl. Phys. Lett. **109**, 052101 (2016), Copyright 2016 AIP].

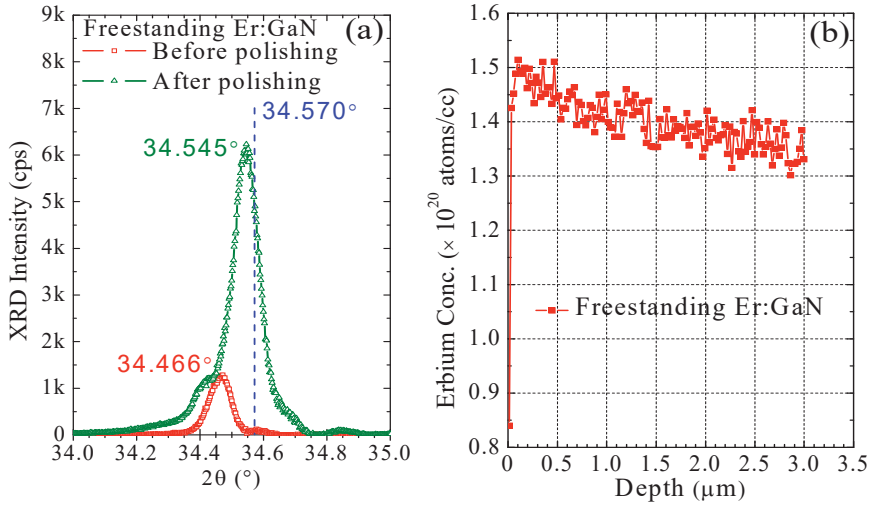

Fig. 2. (a) XRD θ-2θ scans of the GaN (0002) diffraction peak of a freestanding Er:GaN sample before polishing (1.2 mm in thickness) and after double-side polishing (1 mm in thickness). Dashed-line at 34.57º indicates the position of the 2θ diffraction angle of the GaN (0002) peak in strain-free undoped GaN. (b) Er concentration profile in a freestanding Er:GaN probed by SIMS up to 3 μm in depth [Ref. 27, reproduced with permission from Appl. Phys. Lett. **109**, 052101 (2016), Copyright 2016 AIP].

growth of Er:GaN. In HVPE growth, GaCl and $ErCl_3$ were formed by reacting Cl from HCl gas with metallic Ga and Er sources, which were held in two different containers at a temperature of about 1000 °C, serving as the group III and Er dopant sources, respectively. The GaCl and $ErCl_3$ in the vapor phase are transported to the deposition zone by an H_2 carrier gas. Er:GaN is then formed on the GaN/sapphire template by reacting hot gaseous metal chlorides (GaCl and $ErCl_3$) with ammonia gas (NH_3). The substrate temperature was 1030 °C and the growth rate ranged from 10 to 400 μm/hour.

The as-grown wafer of Er:GaN/GaN/sapphire was then processed with LLO to remove the sapphire substrate followed by mechanical and chemical-mechanical polishing on both sample surfaces to obtain a free-standing Er:GaN wafer. Figure 1(a) shows an optical image of a free-standing 2-inch Er:GaN wafer with a thickness 1.2 mm obtained by HVPE (at a growth rate of about 200 μm/hour, grown for 6 hours) before polishing. After polishing, this freestanding Er:GaN wafer had a thickness of 1.0 mm, as shown in Fig. 1(b).

Figure 2(a) compares the X-ray diffraction (XRD) θ-2θ scans of the GaN (0002) diffraction peak of a freestanding Er:GaN sample before and after polishing. Comparison of the peak positions at 34.466º and 34.545º, respectively, for the wafer before and after chemical-mechanical polishing, with the 2θ diffraction peak of strain-free GaN (0002) at 34.57º, reveals the presence of compressive strain in as-grown Er:GaN wafers. However, the smoothing of the surface and removal of shallow defects by chemical-mechanical polishing seem to reduce the stress and curvature in the wafer, as suggested by the observed shift of the 2θ diffraction peak position toward that of strain-free GaN (0002) after wafer polishing. The presence of a slight difference in the peak positions of the 2θ angle between the polished freestanding Er:GaN sample and the strain free GaN is not surprising since the size of Er atom is larger than that of the Ga atom and the majority of Er ions in GaN occupy Ga substitutional sites. To confirm the Er doping concentration (N_{Er}), secondary ion mass spectrometry (SIMS) measurement was performed on a freestanding Er:GaN wafer by Evans Analytical Group (EAG, Inc.). To eliminate the surface effect, the sample's top surface was further polished, reducing the thickness to a few tens of microns. Then, the SIMS profile of the top 3 μm of this polished and smooth surface was measured. In Fig. 2(b), the SIMS results indicate that this sample has an average $N_{Er} = 1.4 \times 10^{20}$ atoms/cm^3.

Figures 3(a) and (b) compare the photoluminescence (PL) emission spectra measured at room temperature for freestanding Er:GaN samples of 1 mm and 11 μm in thicknesses for (a) band-edge non-resonant excitation at λ_{exc} = 375 nm and (b) resonant excitation at λ_{exc} = 980 nm. The strong 1.54 μm peak emission line originating from the intra-4f transition of Er atoms was clearly observed in both cases. The

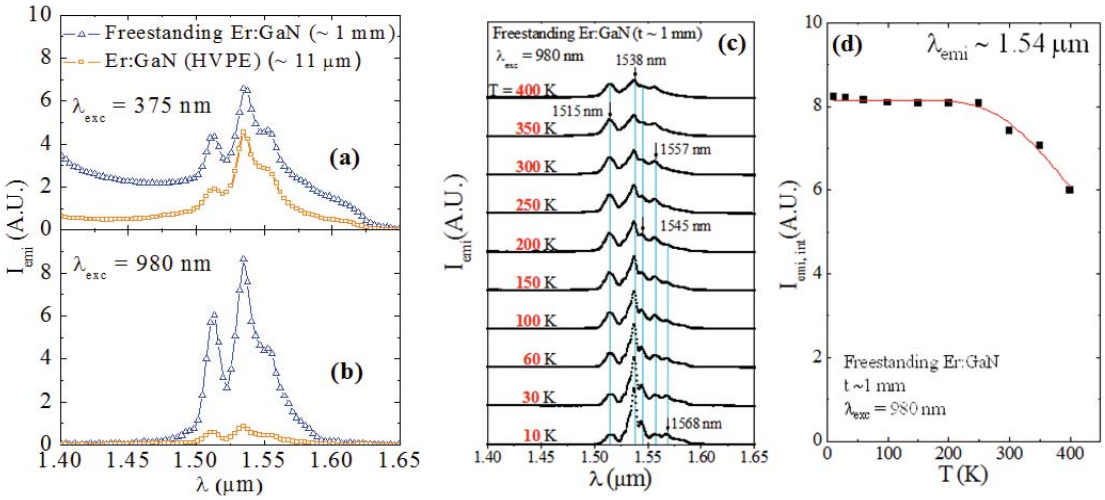

Fig. 3. Comparison of room temperature PL spectra of freestanding Er:GaN samples of two different thicknesses of 1 mm and 11 μm, with (a) band-edge excitation at λ_{exc} = 375 nm and (b) resonant excitation at λ_{exc} = 980 nm. (c) The temperature dependence of the PL spectra of a freestanding Er:GaN sample (1 mm in thickness) under a resonant excitation at λ_{exc} = 980 nm measured between 10 K and 400 K. (d) Integrated PL emission intensity of the 1.54 μm emission of the same freestanding Er:GaN sample as a function of temperature (λ_{exc} = 980 nm) [Ref. 27, reproduced with permission from Appl. Phys. Lett. **109**, 052101 (2016), Copyright 2016 AIP].

measured PL emission spectra under both 375 nm and 980 nm pump wavelengths are quite similar. However, compared to the thin Er:GaN sample which had a thickness of only 11 μm, the freestanding Er:GaN with a thickness of ~ 1 mm exhibits a much stronger PL emission intensity under 980 nm resonant excitation, whereas both thin and thick Er:GaN samples have a comparable PL emission intensity under band-edge non-resonant 375 nm excitation. This can be explained by the fact that the band-edge excitation at 375 nm is predominantly exciting the electron and hole pairs in the GaN host, which has a very small optical absorption length (< 3 μm) [29, 30]. This means that the 375 nm photons are mostly absorbed within the thickness of 6 μm. Therefore, increasing the sample thickness to 1 mm does not further increase optical absorption at 375 nm and PL emission intensity at 1.54 μm. In sharp contrast, 980 nm resonant excitation has an excitation cross section of about 2.2×10^{-21} cm^2 [31] and an optical absorption length > 1 mm. Thus, the 1 mm freestanding Er:GaN wafer takes advantage of large thickness, which allows it to absorb much more of the excitation laser's power at 980 nm than the 11 μm thick wafer. This in turn leads to a much higher emission intensity at 1.54 μm.

The temperature dependence of the PL emission spectra under the 980 nm resonant excitation was measured from 10 K to 400 K to evaluate the thermal quenching effect of the 1.54 μm emission line in a free-standing Er:GaN wafer of 1 mm in thickness and the results are presented in Fig. 3(c). Figure 3(d) plots the PL emission intensity integrated from 1.5 μm to 1.6 μm as a function of the temperature from 10 K to 400 K. There is only a 10% decrease in Er emission near 1.54 μm between 10 K and 300 K, which is consistent with the results seen in Er:GaN thin films [32-34]. The low thermal quenching (10%) of this freestanding Er:GaN material again affirms the promise of Er:GaN for HEL applications.

2. Optical loss measurements of Er:GaN waveguides

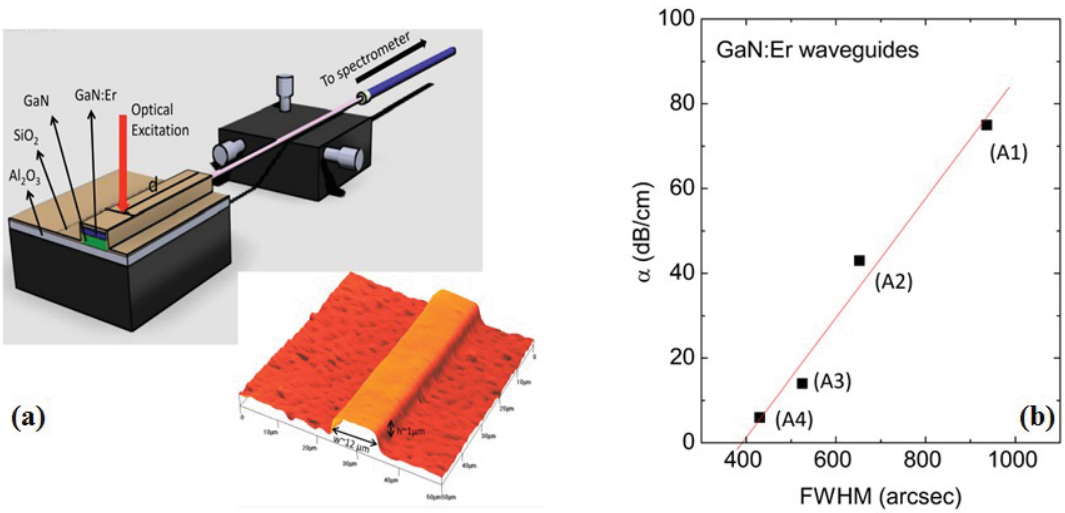

Figure 4 (a) The schematic diagram of the optical attenuation measurement set-up and an AFM image of a Er:GaN waveguide with the waveguide width w ~ 12 μm and height h ~ 1 μm. (b) The optical attenuation coefficient of Er:GaN waveguides as a function of the GaN (002) XRD rocking curve linewidth measured for four different layer structures [after Ref. 35].

Finding ways to measure as well as to understand the mechanisms of optical loss in Er:GaN materials will be vital to provide feedbacks to further improve the materials quality and device structural design. We have constructed a set-up for the optical attenuation measurement, as illustrated in Fig. 4(a) [35]. In the setup, an above band gap excitation or resonant excitation laser diode can be used as an optical excitation light source for the generation of the 1.54 μm emission in the Er:GaN waveguides/rods. The 1.54 μm emission is then collected from the detection end of the Er:GaN waveguides using an optical fiber connected to a thermoelectric (TE) cooled InGaAs infrared spectrometer (Bayspec). As the excitation spot was moved farther away from the detection end of the Er:GaN waveguide with a separation

distance (d), the detected intensity of the 1.54 μm emission decreases exponentially with d as described by $I(d) = I(0)\exp(-\alpha d)$, where I(0) and I(d) refer to the intensities of the 1.54 μm emission at the excitation spot and a distance d away from the excitation spot, respectively, from which the optical attenuation coefficient (α) at 1.54 μm can be obtained.

One of the important results we have obtained is that the effective optical attenuation coefficients of these Er:GaN waveguides depend on the linewidth of the GaN (002) XRD rocking curves in ω-scan. As shown in Fig. 4(b), the optical attenuation coefficient increases almost linearly with an increase of the FWHM of GaN (002) XRD rocking curves. An increase in the FWHM of the XRD rocking curve indicates the presence of a larger number of crystalline dislocations and defects in Er:GaN epilayers due to the use of foreign substrates as well as the incorporation of Er atoms. These embedded crystalline dislocations and defects may play a role as light scattering centers, which explain the correlation between the XRD rocking curve linewidth and optical loss. Our results shown in Fig. 4 reveal that a linewidth ≤ 380 arcsec of GaN (002) XRD rocking curve is required to achieve Er:GaN based waveguides with an optical attenuation coefficient less than 1 dB/cm for the practical applications as a laser gain medium.

3. Characterizing Refractive index of Er:GaN

It is important to characterize the change of index of refraction of Er:GaN due to Er incorporation for the design of various laser structures. GaN is also known to be a uni-axial crystal with a relatively weak birefringence of $\Delta n = n_e - n_o \sim 0.04$ [36-38], where n_e denotes the extraordinary index and n_o the ordinary index. However, our main focus is to investigate, to the first order, the effect of Er doping on the index of refraction of Er:GaN and to verify the potential of Er:GaN for core-cladding laser and amplifier applications.

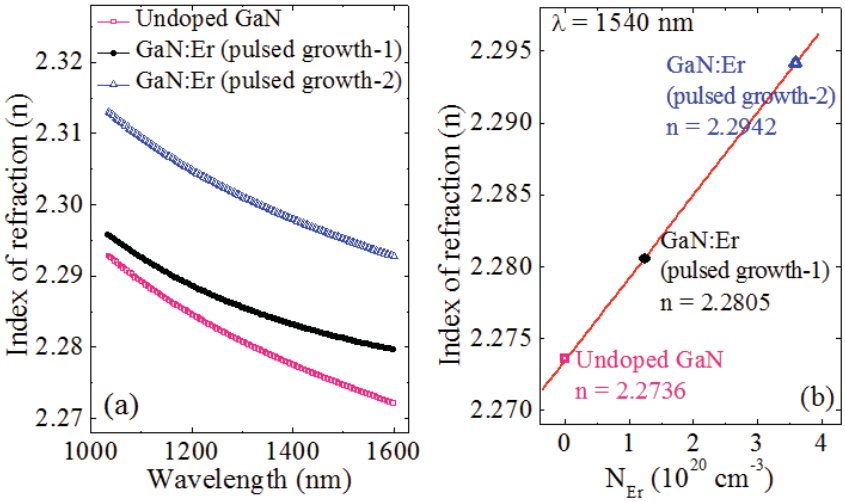

Figure 5. (a) Index of refraction of undoped and Er doped GaN epilayers obtained from fitting spectroscopic ellipsometry data around the IR region; (b) Index of refraction at 1540 nm plotted as a function of Er concentration (N_{Er}) [Ref. 40, reproduced with permission from Appl. Phys. Lett. **105**, 081104 (2014), Copyright 2014 AIP].

The changes in the refractive index due to Er incorporation were measured by spectroscopic ellipsometry (alpha-SE Ellipsometer by J.A. Woollam Company) [40]. To ensure the reliability of the measurement results, the refractive index values of the undoped GaN (n_o) were compared to a previous published result [39] as well as with the reference data supplied with the spectroscopic ellipsometry (SE) system. The results shown in Fig. 5 indicate that the measurement results for undoped GaN are consistent with the reference values obtained using the same SE measurement technique [39]. Moreover, the raw SE data were fit over a wide spectral range (385 nm - 1600 nm) which adds confidence to the determined optical constants.

In Fig. 5(a), we show the measured index of refraction values (n) in the infrared spectral region for an undoped GaN and the two Er doped GaN epilayers grown by MOCVD [40]. The results indicate that n increases with an increase of the Er doping concentration (N_{Er}) at all wavelengths. Since 1.54 μm is the

wavelength of most interest, we plot the values of n at 1.54 μm as a function of N_{Er} for these samples, a linear relationship between n_{Er} and N_{Er} is obtained, as shown in Fig. 5(b),

$$n = n_o + b\, N_{Er} \quad (1)$$

where the fitted values of $n_0 = 2.2735$ and $b = 0.00575 \times 10^{-20}$ cm^3. Knowing this linear dependence will aid in the design of lasers based on Er:GaN. More importantly, the increase of index of refraction stresses the potential use of Er:GaN as an optical gain medium operating at 1.54 while un-doped GaN could be employed as a nearly lattice matched cladding layers.

4. Enhancement of 1.5 μm emission under 980 nm resonant excitation in Er and Yb co-doped GaN epilayers

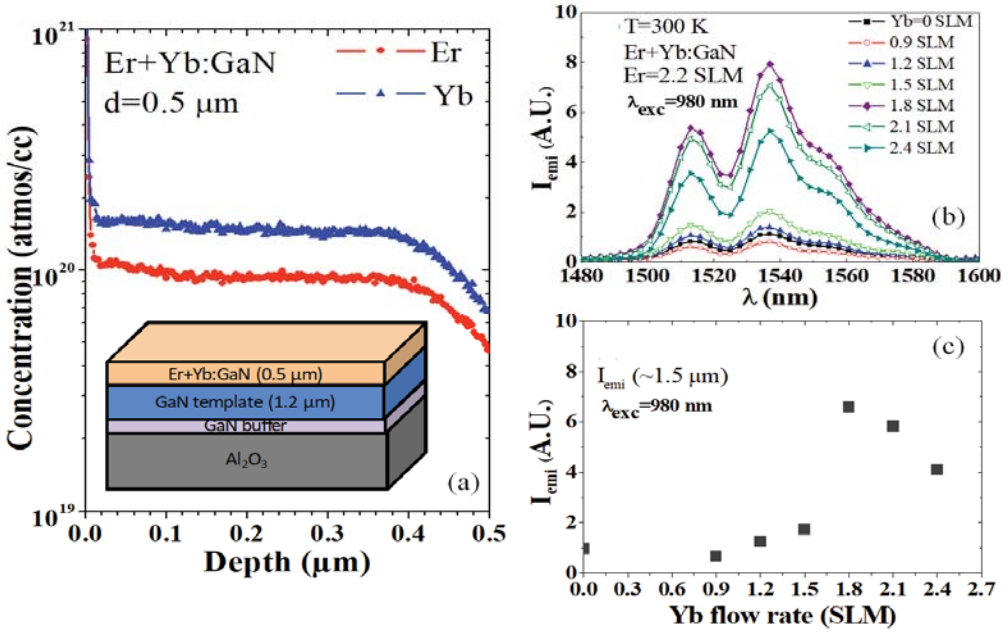

Figure 6. (a) SIMS profiles of Er and Yb concentrations in an Er+Yb:GaN epilayer grown under a Yb flow rate of 1.8 SLM and Er flow rate of 2.2 SLM. The inset is a schematic structure of Er+Yb:GaN epilayers used in this study. (b) Room temperature PL spectra of Er+Yb:GaN epilayers under 980 nm resonant excitation. (c) Integrated PL intensity near 1.5 μm (integrated from 1.48 to 1.6 μm) as a function of the Yb flow rate under 980 nm resonant excitation (λ_{exc}= 980 nm) [Ref. 25, reproduced with permission from Appl. Phys. Lett. **109**, 152103 (2016), Copyright 2016 AIP].

It has been well established that Er and ytterbium (Yb) co-doping in a solid host is an effective approach to enhance the Er emission at 1.5 μm under 980 nm resonant excitation [41-46]. This is due to the fact that the absorption cross section of Yb^{3+} at 980 nm is about one order of magnitude larger than that of Er^{3+}. In Er and Yb co-doped materials, Yb^{3+} ions act as sensitizers by absorbing 980 nm excitation photons and then transferring energy resonantly from their excited $^2F_{5/2}$ state to the $^4I_{11/2}$ level of Er^{3+} ions [41-46]. This efficient resonant energy transfer process is facilitated by the close match between the energy levels of the $^2F_{5/2}$ state of Yb^{3+} and the $^4I_{11/2}$ state of Er^{3+}. This transfer is then followed by a rapid nonradiative decay to the first $^4I_{13/2}$ excited manifold of Er^{3+} ions, after which a direct transition to the $^4I_{15/2}$ ground state of Er^{3+} occurs, resulting in the 1.5 μm emission [46]. The incorporation of Yb at a doping level similar to that of Er is thus expected to provide a nearly one order of magnitude enhancement in the effective optical absorption efficiency at 980 nm and hence a higher emission efficiency at 1.5 μm [46].

We have carried out the in-situ synthesis of Er and Yb co-doped GaN epilayers (Er+Yb:GaN) using MOCVD [25]. To obtain Er+Yb:GaN epilayers, Er flow rate was set at a value of 2.2 SLM (standard liters

per minute) and the Yb flow rate was varied from 0.9 to 2.4 SLM with an increment of 0.3 SLM. XRD was used to characterize the influence of Yb incorporation on the crystalline quality of Er+Yb:GaN epilayers. The inset of Fig. 6(a) shows the schematic structure of the RE doped GaN epilayers (Er+Yb:GaN). SIMS was performed by Evans Analytical Group (EAG, Inc.) to probe the Er and Yb concentration profiles in Er+Yb:GaN epilayers. For instance, for an Er+Yb:GaN epilayer grown under a Yb flow rate of 1.8 SLM and an Er flow rate of 2.2 SLM, SIMS results shown in Fig. 6(a) revealed that the concentrations of Er and Yb are quite uniform throughout the crystal and are about $1.0x10^{20}$ and $1.5x10^{20}$ atoms/cm^3, respectively. The expected major benefit of Yb and Er co-doping is the enhancement of the absorption efficiency at 980 nm via the sensitization effect [41-46]. Room temperature PL spectra of the same set of Er+Yb:GaN epilayers grown under varying Yb flow rates from 0 to 2.4 SLM and a fixed Er flow rate of 2.2 SLM were measured under 980 nm resonant excitation and the results are presented in Fig. 6(b). For the Yb flow rates below 1.0 SLM, there is no gain in the Er related emission intensity at 1.5 μm in Er+Yb:GaN over Er:GaN. The improvement in the 1.5 μm emission intensity in Er+Yb:GaN epilayers over Er:GaN epilayers becomes gradually visible when the Yb flow rate is increased beyond 1.0 SLM. The integrated emission intensity near 1.5 μm is plotted in Fig. 6(c) as a function of the Yb flow rate. It is clear that the Er related emission intensity at 1.5 μm reaches a maximum enhancement factor of 7 when the Yb flow rate was at 1.8 SLM, beyond which a further increase in the Yb flow rate resulted in a reduction in the emission intensity at 1.5 μm. This behavior could be related to a reduction in the crystalline quality or Yb ion-ion cluster formation at higher Yb flow rates. However, the observed enhancement in the 1.5 μm emission efficiency in MOCVD grown Er+Yb:GaN epilayers over Er:GaN epilayers is consistent with the expected sensitization effect [41-46]. The results point to an effective way to improve the emission efficiency of Er doped GaN for optical amplification and lasing applications under optical pump using 980 nm light.

5. Excitation and emission mechanisms of low quantum defect lasing in Er:GaN in 1.5 μm spectral region

The energy levels of the $^4I_{13/2}$ first excited state and the $^4I_{15/2}$ ground state manifolds of Er^{3+} ions in Er:YAG and hence the excitation and emission schemes of Er:YAG eyesafe lasers are now very well understood [6-13]. The most common resonant excitation lines in Er:YAG are at 1470 nm and 1533 nm to achieve, respectively, a quasi-four-level and quasi-three-level system, while the emission lines occur at 1645 and 1617 nm. Although the 4f-shell of trivalent Er^{3+} is mostly insensitive to the host material, previous theoretical and experimental studies have indicated that the local arrangements of atoms in the nearest neighborhood of the Er^{3+} ion can affect the details in the optical absorption and emission spectrum [47]. This implies that the excitation and emission energy level scheme of Er:YAG lasers may not be entirely applicable to attain Er:GaN lasers.

We have performed optical absorption and resonantly excited photoluminescence emission spectroscopy studies on freestanding Er:GaN quasi-bulk crystals with aim to construct the energy level diagrams pertaining to the excitation and emission mechanisms of Er:GaN eyesafe HEL [28]. Freestanding Er:GaN crystals of 1 mm in thickness were obtained via growth by HVPE in conjunction with a laser-lift-off process. The samples were then subjected to double side chemical-mechanical polishing. The final thickness of the sample used in this study was 600 μm. A broad light source covering a wavelength range between 170 and 2100 nm coupled with a triple grating monochromator was used as a variable wavelength excitation source for the optical absorption measurements. The absorption setup provides an overall spectral resolution of 2 nm. Figure 7(a) shows the room temperature optical absorption spectrum measured in the 1450 - 1650 nm region. The spectrum revealed two dominant absorption bands near 1514 nm and 1539 nm. Fitting the absorption spectrum using a multiple Gaussian peak fitting also resolved a third peak near 1556 nm. Figure 7(b) shows the PL emission spectrum of the same Er:GaN sample measured at 250 K around 1.5 μm. The excitation source is a 980 nm laser diode and the PL signal was collected using an InGaAs detector in conjunction with a spectrometer. The spectral shape of the PL spectrum shown in Fig. 7(b) is rather similar to that of the absorption spectrum shown in Fig. 7(a) with a central peak near 1538 nm, but with additional fine features resulting from the transitions between Stark sublevels in the $^4I_{15/2}$ ground state and the $^4I_{13/2}$ first excited state manifolds, which were not resolved in the optical absorption spectrum.

A significant result is that there are nearly no features and the absorption/emission is extremely low below 1500 nm. This is in sharp contrast to the fact that Er^{3+} in most other host materials such as YAG and

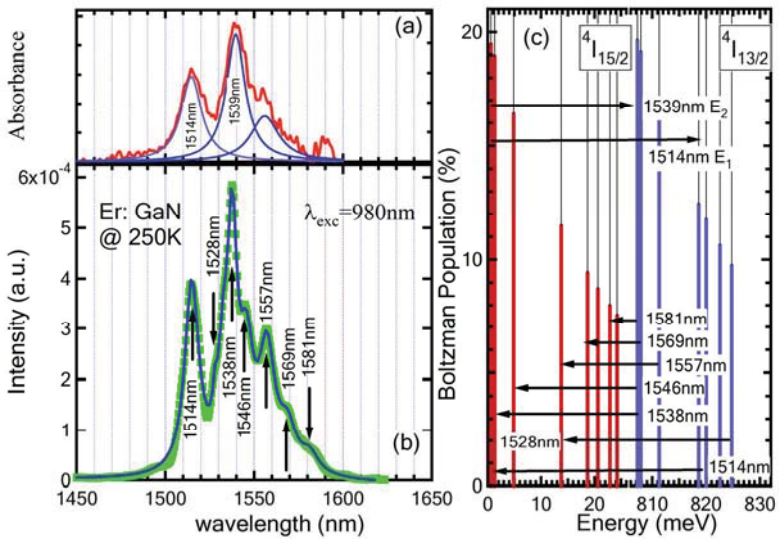

Figure 7. (a) Optical absorption spectrum of an Er:GaN freestanding quasi-bulk crystal measured in the 1.5 μm spectral region with 2 nm spectral resolution. (b) PL emission spectrum of the same sample measured in the 1.5 μm spectral region with excitation wavelength λ_{exc} = 980 nm. (c) Energy level diagram of Er^{3+} in the ground ($^4I_{15/2}$) and first excited ($^4I_{13/2}$) state manifolds in Er:GaN re-constructed from Ref. 47. The observed absorption lines from (a) and emission lines from (b) are indicated by arrows. The corresponding 300 K Boltzmann occupation factors for each energy level are indicated by the vertical bold solid lines [Ref. 28, reproduced with permission from Appl. Phys. Lett. **111**, 072109 (2017), Copyright 2017 AIP].

silica glass exhibit a strong absorption line near 1470 nm, corresponding to a resonant transition between Stark sublevels, from the bottom of the $^4I_{15/2}$ ground state manifold to the top of the $^4I_{13/2}$ first excited state manifold. This transition line near 1470 nm is the most common pumping line employed for achieving Er:YAG lasers. In fact, the spectra shown in Fig. 7 are in excellent agreement with the results of a previous crystal field analysis [47], based on which the energy level diagram of Er^{3+} in the ground ($^4I_{15/2}$) and first excited ($^4I_{13/2}$) state manifolds in Er:GaN has been constructed as shown in Fig. 7(c). The experimentally observed transition energies in Figs. 7(a) and (b) are indicated by the arrows in Fig. 7(c).

We have also measured the PL emission spectra excited by laser diodes with operating wavelengths tuned into the resonant excitation closely matching with the optical absorption maxima near 1514 and 1539 nm. The PL emission spectra under 1514 nm and 1540 nm excitation are shown in Fig. 8(a) and Fig. 8(b), respectively. Multiple emission lines resulting from the transitions between the Stark sublevels in the $^4I_{15/2}$ ground state and the $^4I_{13/2}$ first excited state manifolds have been resolved, with several lines have been identified in the PL spectrum shown in Fig. 8(b) under 980 nm pump. Under resonant excitations, the

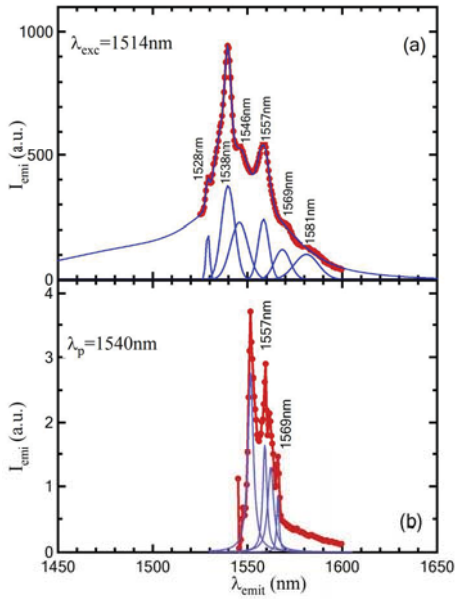

Figure 8. Resonantly excited emission spectra measured near 1.5 μm of an Er:GaN freestanding quasi-bulk crystal with (a) λ_{exc} = 1514 nm and (b) λ_{exc} = 1541 nm [Ref. 28, reproduced with permission from Appl. Phys. Lett. **111**, 072109 (2017), Copyright 2017 AIP].

most common emission lines beyond 1550 nm appear to be near 1557 nm, 1569 nm and 1581 nm. It is interesting to note that the emission peaks become narrower as the resonant pump wavelength increases and the PL spectrum under 1540 nm pump composed of sharpest lines. The fitted full width at half maximum (FWHM) of deconvolution Gaussian peaks is as narrow as 0.1 nm for the PL spectrum under 1540 nm excitation. This is understandable because the recombination under resonant excitation using longest wavelength excites the least number of sublevels and involves the least steps of thermal relaxation processes and so the FWHM of emission lines approaches the true intrinsic characteristics of intra-4f shell transitions.

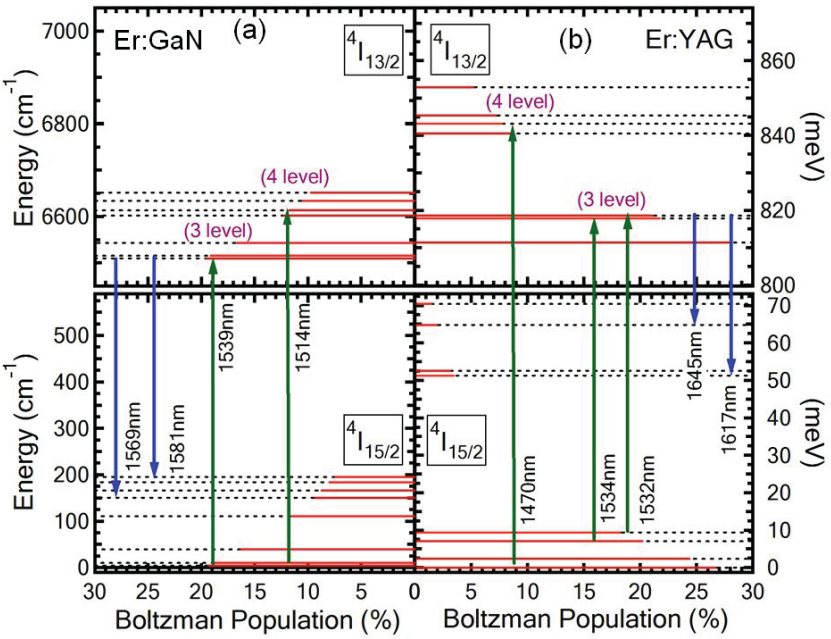

Figure 9. (a) Energy level diagram constructed from the results of Figs. 7 and 8, providing the excitation and emission mechanisms of Er:GaN low quantum defect lasers operating near 1.5 μm. (b) The equivalent energy level diagram of Er:YAG lasers. 4 level and 3 level indicate, respectively, a quasi-four-level and quasi-three-level system. The corresponding 300 K Boltzmann occupation factors for each energy level are indicated by the horizontal bold solid lines [Ref. 28, reproduced with permission from Appl. Phys. Lett. **111**, 072109 (2017), Copyright 2017 AIP].

One of the criteria for achieving lasing is to attain population inversion, which can be reached more easily if the upper laser level is easily populated, whereas the lower laser level is rapidly depopulated. With this in mind together with the observed optical absorption and emission lines, we have constructed in Fig. 9(a) the energy level diagram of the ground and first excited states to illustrate the most likely excitation and lasing scenarios in resonantly pumped eyesafe Er:GaN lasers. The energy levels clearly show that the most appropriate pump lines appear to be 1514 nm and 1539 nm, whereas the lasing emission lines most likely to occur at 1569 nm and 1581 nm. For comparison, we also plotted the corresponding energy level diagram illustrating the well understood excitation and lasing schemes in resonantly pumped eyesafe Er:YAG lasers in Fig. 9(b). It can be seen that the differences between the pumping and lasing wavelengths in Er:GaN are smaller than those in Er:YAG for both the quasi-four-level and quasi-three-level lasing systems, implying that resonantly pumped eyesafe Er:GaN lasers potentially possess smaller quantum defects than those based on Er:YAG. Another potential advantage of Er:GaN is its expected lasing wavelength occurring below 1600 nm. It is known that the current state-of-the-art near IR tracking cameras used in eyesafe HEL systems are based on GaInAs epitaxial structures grown on lattice-matched InP [48], which have a bandgap of 0.75 eV and a cut-off wavelength of 1620 nm, making GaInAs tracking cameras less sensitive and hence more difficult to track the lasing wavelengths of Er:YAG than those of Er:GaN.

III. SUMMARY

Freestanding wafers of Er:GaN were obtained via HVPE growth in conjunction with a laser-lift-off process. Optical loss measurements revealed that achieving Er:GaN crystals with a GaN (002) XRD rocking curve linewidth of ≤ 380 arcsec will be desirable for providing a low optical loss (< 1 dB/cm) for practical applications of slab, waveguide or rod lasers. It was also shown that the index of refraction (n) of Er:GaN increases linearly with Er concentration (N_{Er}) following $n = n_o + b N_{Er}$ with the measured value of b = 0.00575 x 10^{-20} cm^3. This finding confirms the potential of Er:GaN for the construction of core-cladding laser structures and single crystal core-cladding fiber laser structures based on GaN/Er:GaN/GaN multilayer structures, in which Er:GaN is the gain medium and un-doped GaN could be employed as a nearly lattice matched cladding layer. Optical absorption and resonantly excited photoluminescence emission spectra have enabled the construction of energy level diagrams pertaining to the excitation and emission mechanisms of Er:GaN eyesafe HELs operating around 1550 nm and the results have shown that the common excitation and emission scheme of Er:YAG is not applicable to achieve Er:GaN eyesafe lasers. In addition to higher thermal conductivity of Er:GaN over Er:YAG gain medium, Er:GaN eye-safe lasers appear to possess lower quantum defects than Er:YAG lasers.

The work is supported by High Energy Laser Joint Technology Office (grant #N00014-17-1-2531) monitored by Sarwat Chappell of ONR. Lin and Jiang would also like to acknowledge the support of Whitacre Endowed Chairs by the AT & T Foundation.

REFERENCES

a) jingyu.lin@ttu.edu; hx.jiang@ttu.edu

[1] E. Desurvire, Erbium-doped Fibre Amplifiers: Principles and Applications, John Wiley & Sons, 1994.
[2] M. J. Connelly, Semiconductor Optical Amplifiers, Springer, 2002.
[3] Y. Kalisky and O. Kalisky, Opt. Eng. **49**, 091003 (2010).
[4] J. A. Zuclich, D. J. Lund, and B. E. Stuck, Health Phys. **92**, 15 (2007).
[5] J. Bailey, A. Simpson, and D. Crisp, Publications of the Astronomical Society of the Pacific, **119**, 852 (2007).
[6] Y. X. Fan and R. G. Schlecht, US patent 4,995,046 (1991).
[7] N. Ter-Gabrielyan, V. Fromzel, X. Mu, H. Meissner, and M. Dubinskii, Opt. Lett. **38**, 2432 (2013).
[8] K. Spariosu, V. Leyva, R. A. Reeder, and M. J. Klotz, IEEE J. Quantum Electronics, **42**, 182 (2006).
[9] J. O. White, IEEE J. Quantum Electronics, **45**, 1213 (2009).
[10] N. Ter-Gabrielyan, V. Fromzel, X. Mu, H. Meissner, and M. Dubinskii, Optics Letters, **38**, 2432 (2013).
[11] M. Němec, J. Šulc, L. Indra, M. Fibrich and H. Jelínková, Laser Physics, 25, 115 (2014).
[12] T. Sanamyan, J. Optical Society of America B, 33, D1 (2016).
[13] D. J. Ottaway, L. Harris, and P. J. Veitch, Optics Express, 24, 15341 (2016).
[14] G. Huber, C. Krankel, and K. Petermann, J. Opt. Soc. Am. **27**, B93 (2010).
[15] W. Koechner "Solid-state laser engineering", 5th edition, Spring-Verlag, Berlin Heidelberg, (1999).
[16] J. Vetrovec, "Solid-state high-energy laser," Proc. SPIE on Laser and Beam Control Technologies **4632**, 104 (2002).
[17] A. Giesen and J. Speiser, IEEE J. Selected Topics in Quantum Electronics, **13**, 598 (2007).
[18] S. Nakamura, G. Fasol, and S. J. Pearton, The Blue Laser Diode: The Complete Story (Springer, New York, 2000).
[19] A. Bergh, G. Crawford, A. Duggal, and R. Haitz, Phys. Today, **54**, 42 (2001).
[20] Y. Narukawa, M. Sano, M. Ichikawa, S. Minato, T. Sakamoto, T. Yamada, and T. Mukai, Japn J. Appl. Phys. Part 2 Letters, **46**, 963, (2007).
[21] J. Day, J. Li, D. Lie, C. Bradford, J. Lin, and H. Jiang, Appl. Phys. Lett., **99**, 031116 (2011).
[22] H. Shibata, Y. Waseda, H. Ohta, K. Kiyomi, K. Shimoyama, K. Fujito, H. Nagaoka, Y. Kagamitani, R Simura and T. Fukuda, Materials Transactions **48**, 2782 (2007).
[23] R. Hui, Y. Wan, J. Li, S. Jin, J. Y. Lin, and H. X. Jiang, IEEE J. Quantum Electronics, **41**, 100 (2005).

[24] T. M. Al tahtamouni, M. Stachowicz, J. Li, J. Y. Lin, and H. X. Jiang, Appl. Phys. Lett. **106**, 121106 (2015).
[25] Q. W. Wang, J. Li, J. Y. Lin, and H. X. Jiang, Appl. Phys. Lett. **109**, 152103 (2016).
[26] D. W. Jeon, Z. Y. Sun, J. Li, J. Y. Lin, and H. X. Jiang, Optical Materials Express **5**, 596 (2015).
[27] Z. Y. Sun, J. Li, W. P. Zhao, J. Y. Lin, and H. X. Jiang, Appl. Phys. Lett. **109**, 052101 (2016).
[28] Z. Y. Sun, L. C. Tung, W. P. Zhao, J. Li, J. Y. Lin, and H. X. Jiang, Appl. Phys. Lett. **111**, 072109 (2017).
[29] A. Braud, RE excitation processes in GaN, Chapter 8 in Rare-earth doped III-Nitrides for Optoelectronic and Spintronic Applications, edited by K. O'Donnell and V. Dierolf, published by Canopus Academic Publishing Ltd and Springer SBM (2010).
[30] I. W. Feng, Jing Li, J. Y. Lin, H. X. Jiang and J. Zavada, "Optical excitation cross section of erbium in GaN," Applied Optics **52**, 61132 (2013).
[31] R. Hui, R. Xie, I. W. Feng, Z. Y. Sun, J. Y. Lin, and H. X. Jiang, Appl. Phys. Lett. **105**, 051106 (2014).
[32] P. N. Favennec, H. L'Haridon, M. Salvi, D. Moutonnet, and Y. Le Guillou, Electron. Lett. **25**, 718 (1989).
[33] A. J. Steckl and J. M. Zavada, MRS Bull. **24**, 33 (1999).
[34] C. Ugolini, N.Nepal, J. Y. Lin, H. X. Jiang, and J. M. Zavada, Appl. Phys. Lett. **89**, 151903 (2006).
[35] I. W. Feng, W. P. Zhao, J. Li, J. Y. Lin, H. X. Jiang, and J. Zavada, "Correlation between the optical loss and crystalline quality in erbium-doped GaN optical waveguides," Applied Optics **52**, 5426 (2013).
[36] S. R. Bowman, C. G. Brown, M. Brindza, G. Beadie, J. K. Hite, J. A. Freitas, C. R. Eddy, J. R. Meyer, and I. Vurgaftman, Opt. Mater. Express **4**, 1287 (2014).
[37] S. Shokhovets, M. Himmerlich, L. Kirste, J. H. Leach, and S. Krischok, Appl. Phys. Lett. **107**, 092104 (2015).
[38] R. Hui, Y. Wan, J. Li, S. X. Jin, J. Y. Lin, and H. X. Jiang, Appl. Phys. Lett. **83**, 1698 (2003).
[39] G. Yu, G. Yu, G. Wang, H. Ishikawa, M. Umeno, T. Soga, T. Egawa, J. Watanabe, and T. Jimbo, Appl. Phys. Lett., **70**, 3209 (1997).
[40] S. Alajlouni, Z. Y. Sun, J. Li, J. M. Zavada, J. Y. Lin, and H. X. Jiang, "Refractive index of erbium doped GaN thin films," Appl. Phys. Lett. **105**, 081104 (2014).
[41] G. Huber, C. Krankel, and K. Petermann, "Solid-state lasers: status and future", J. Opt. Soc. Am. **27**, B93 (2010).
[42] V. Prajzler, Z. Burian, I. Hüttel, J. Špirková, J. Hamáček, J. Oswald, J. Zavadil, and V. Peřina, Acta Polytechnica, **46**, 49 (2006).
[43] I. B. Gallo, A. Braud, A. R. Zanatta, Optics Express **21**, 28394 (2013).
[44] C. Strohhöfer and A. Polman, Optical Materials, **21**, 705 (2003).
[45] K. Uwai, H. Nakagome, and K. Takahei, Appl. Phys. Lett. **50**, 977 (1987).
[46] C. Grivas, Progress in Quantum Electronics, **45-46**, 3 (2016).
[47] M. Stachowicz, A. Kozanecki, C. G. Ma, M. G. Brik, J. Y. Lin, H. X. Jiang, and J. M. Zavada, Optical Materials **37**, 165 (2014).
[48] A. Rogalski, Infrared Physics & Technology **43**, 187 (2002).